LANGMUIR

Tunable Omnidirectional Antireflection Coatings Inspired by Inclined Irregular Nanostructures on Transparent Blue-Tailed Forest Hawk Dragonfly Wings

Yu-Han Chen, Huei-Yin Chen, Chung-Jui Lai, Jung-Hsuan Hsu, Kun-Yi Andrew Lin,* and Hongta Yang*

Read Online

ACCESS | Metrics & More | Article Recommendations | Supporting Information
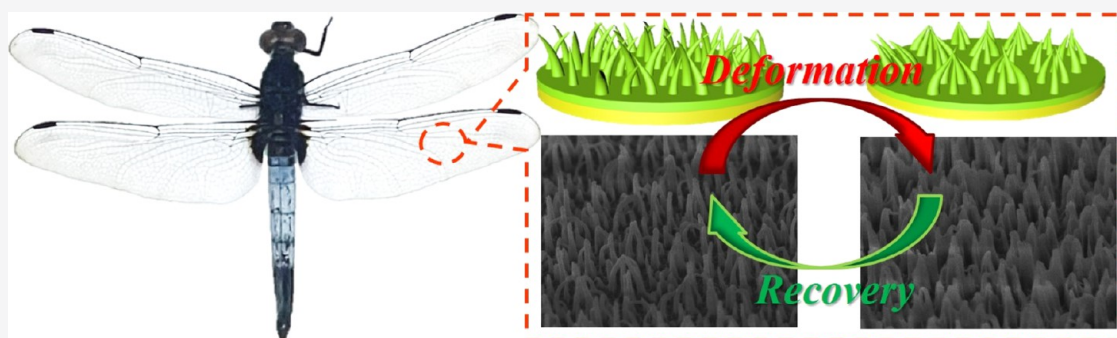
ABSTRACT: Randomly arranged inclined irregular nanostructure-covered blue-tailed forest hawk dragonfly wings are highly transparent for wide viewing angles. Inspired by the dragonfly wings, monolayer silica colloids are self-assembled on shape memory polymer-coated substrates and utilized as plasma etching masks to pattern disorderly arranged inclined irregular conical structures. The structures build gradual refractive index transitions at various angles of incidences, resulting in omnidirectional antireflection performance over the whole visible wavelength region. In comparison with a bare substrate, the optimized structure-covered substrate presents 10% higher optical transmission at 0° and even 41% higher optical transmission at an angle of incidence of 75°. Importantly, by manipulating the structural configuration of the shape memory polymer-based structures, the corresponding antireflection characteristics can be instantaneously and reversibly eliminated and recovered after drying out of common household liquids or applying contact pressures in ambient environments. The tunable omnidirectional antireflection coatings are prospective candidates for realizing optical modulation, which exhibits an enormous application value in smart windows, intelligent display screens, optical components, and novel optoelectronic devices.

INTRODUCTION

Polymer coatings with appropriate refractive indices and thicknesses are able to moderate the abrupt change of refractive index between two different media, which minimize Fresnel reflection and translate the reflected light into increasing transmission.[1] As a result, the antireflection coatings have been extensively employed to reduce veil glare, eliminate ghost images, protect image readability, and improve contrast for diverse optical applications.[2−5] Although polymers are adequate for large-areal processing and easily adhered to flexible substrates, low-refractive-index polymers are rare and expensive. To overcome the challenges, a variety of methodologies, such as phase separation, plasma-enhanced chemical vapor deposition, sol−gel process, multilayer deposition of nanoparticles, and integration of voids using hollow particles, have been developed to build antireflection coatings possessing homogeneously distributed pores much smaller than visible wavelengths for reducing refractive indices.[6−14] Nevertheless, it

is further necessary to create a refractive index gradient for achieving broad-band antireflective characteristics.

Over 4 million years of evolution, biological systems have developed diverse nanometer-scale architectures to bring about unique functionalities.[15−17] For instance, hawk moths, glasswing butterflies, and cicadas use hexagonally non-close-packed subwavelength conical structure arrays for suppressing reflectivity from their wings to avoid tracking by predators.[18−20] Interestingly, dragonfly wings, covered with disorderedly arranged subwavelength-inclined conical structures, can
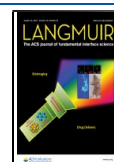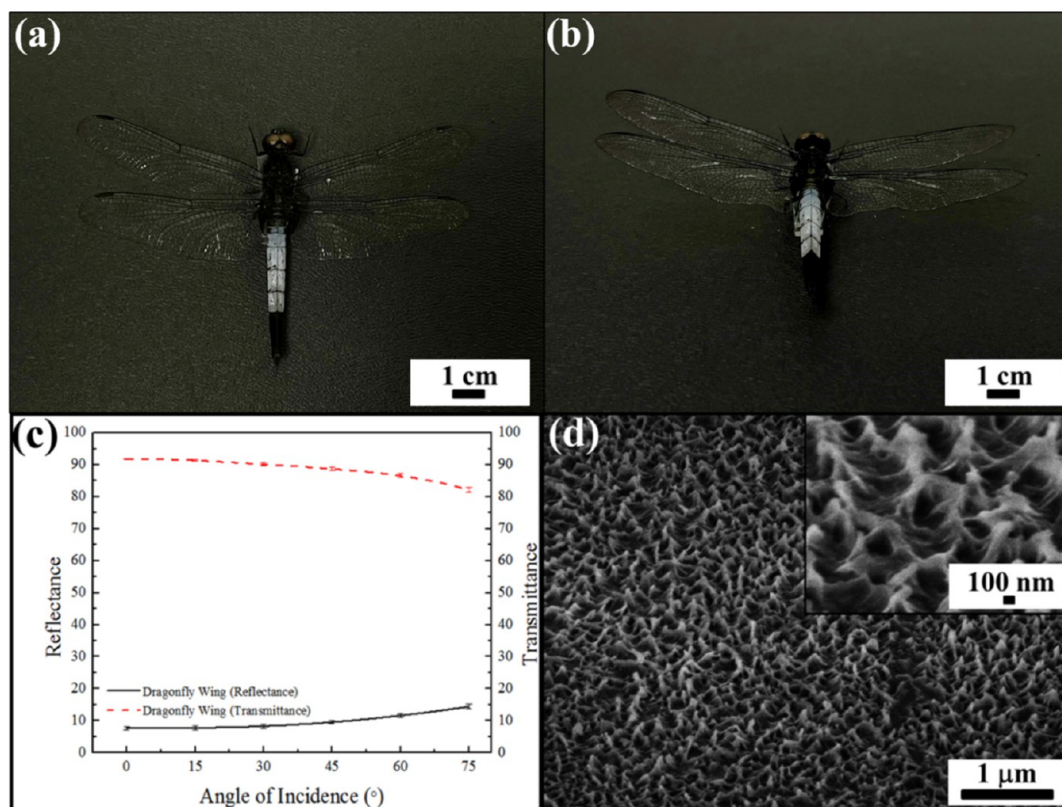
Figure 1. Photographic images of a blue-tailed forest hawk dragonfly taken at (a) 0 and (b) 60°. (c) Average optical reflectances and average optical transmittances in the visible wavelength region acquired from the dragonfly wing at various incident angles. (d) Tilted-view SEM image of the dragonfly wing in (a).

even overcome dazzling of wings by sunlight during flying.[21] These conical structures establish graded refractive index transitions over wide angles of incidence, resulting in broadband omnidirectional antireflection behaviors and minimized light scattering on the transparent wings.

Inspired by the insect wings, a variety of nanocones, nanodomes, nanopillars, nanoholes, and nanopyramids, have been created to serve as antireflective structures.[22−26] Nevertheless, the unwanted reflective losses of most nanostructures are rapidly increased with increasing viewing angles. Therefore, it is of great significance for creating inclined nanostructures to realize omnidirectional antireflection coatings, though it is still a challenge in fabricating the structures using current lithography-based methodologies, such as interference lithography, nanoimprint lithography, and electron beam lithography.[27−29] Fueled by the considerable progress of self-assembly technologies, colloidal lithography renders an alternative to design and build antireflective nanostructures. In comparison with traditional bottom-up methodologies, a spin-coating technology has recently been developed to self-assemble monolayer non-close-packed silica colloids, which serve as lithography masks to engineer nanostructures.[30] It is obvious that the non-close-packed arrangement provides more interspace for constructing inclined nanostructures and is critical to mimic the antireflective architectures on the dragonfly wings.

Shape memory materials can regain their original shapes and alternate their molecular configurations in response to external stimuli, including magnetic field, electric field, heat, light, potential of hydrogen, and solvent.[31−37] In comparison with conventional shape memory metal alloys, shape memory polymers are widely utilized because of their lightweight, lower cost, high shape deformability, and good manufacturability.[38] Benefiting from the rapid development of shape memory polymers, diversified tunable nanostructures are designed and constructed as antireflection coatings.[39,40] The nanostructures are capable of being deformed at will and reconstructed after deformation to reversibly switch the corresponding antireflective characteristics triggered by external stimuli, which provide a platform for developing intelligent optical and optoelectronic devices. However, the physical stimuli-responsive shape recoveries are time-consuming, significantly restricting their uses in numerous applications that require rapid response.[41,42] In contrast, chemical stimuli-responsive shape memory polymers can modulate intermolecular forces and revert to their original configurations instantly by applying specific solvents.[43,44] Nevertheless, most of the solvents cause serious corrosion of other device components and further pose environmental hazards. Moreover, shape memory-inclined antireflective nanostructures have not yet been reported, impairing the development of tunable omnidirectional broadband antireflection coatings.

Herein, we report subwavelength shape memory-inclined conical structures, which biomimic the antireflective structures covering dragonfly wings, by integrating a colloidal lithography approach and a new pressure-responsive shape memory polymer. Monolayer non-close-packed silica colloids are self-assembled on the shape memory polymer, followed by a dry etching process to engineer inclined nanostructures. The nanostructures behave impressive broad-band antireflective characteristics over wide viewing angles. In comparison with traditional antireflection coatings, this new type of shape
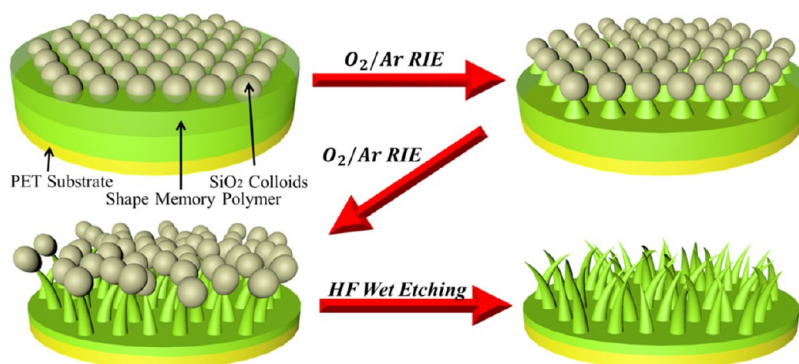
Figure 2. Schematic illustration of the fabrication process for engineering inclined conical structures.

memory antireflective nanostructures can further adjust their antireflection performances instantaneously by applying either small contact pressures or common household liquids (e.g., water and ethanol) under ambient conditions. Moreover, the corresponding antireflection features can be memorized even after removing the external stimuli. In this study, we systematically evaluate the antireflective characteristics of the dragonfly wing-inspired inclined nanostructures for bridging the gap between practical applications and theoretical design.

■ EXPERIMENTAL SECTION

Assembly of Monolayer Silica Colloids with Non-close-Packed Arrangement by Spin Coating. The standard Stöber approach was adopted to hydrolyze tetraethyl orthosilicate (98 vol %, Sigma-Aldrich) in an ethanol (200 proof, Sigma-Aldrich) solution, in the presence of ammonium hydroxide (28 vol %, Thermo Fisher Scientific) as a catalyst, for synthesizing monodispersed silica colloids with diameters of 190, 140, and 90 nm.[45] After removing the catalyst and synthetic byproducts in five centrifugation and dispersion cycles, the purified colloids were re-dispersed in a photocurable oligomer mixture, consisting of ethoxylated trimethylolpropane triacrylate (ETPTA, Sartomer) oligomers, (ethylene glycol)diacrylate (EGDA, Sartmer) oligomers, and 2-hydroxy-2-methyl-1-phenyl-1-propanone (HMPP, Darocur 1173, BASF) as a photoinitiator. The volumetric fractions of colloids, ETPTA oligomers, EGDA oligomers, and HMPP in the silica colloidal suspension were controlled to be 20 , 20, 59, and 1 vol %. Poly(ethylene terephthalate) (PET, Wisegate Technology) films employed in the assembly procedure were coated with poly(ETPTA)/poly(EGDA) composite layers, in which the volume ratio of poly(ETPTA) to poly(EGDA) was 1:3. The as-prepared suspension was filtered to eliminate any aggregated silica colloids and then deposited onto the composite layer-coated PET substrate. Afterward, the substrate was spun at 2000 rpm for 2 min, 4000 rpm for 2 min, and 8000 rpm for 6 min using a spin coater (WS-400B-6NPP-Lite, Laurell Technologies), while the colloids were assembled into a non-close-packed arrangement. A UV curing system (X Lite, OPAS) was finally used for photopolymerizing the oligomer mixture.

Templating Nanofabrication of Conical Structures by Colloidal Lithography. Oxygen/argon plasma etching of the monolayer silica colloid/polymeric composite-coated PET substrate was implemented on an ICP reactive ion etcher (Vision 320, Advance Vacuum) to directly pattern conical structures. The reactive ion etchings (RIE) were carried out by applying a mixture of oxygen (10 to 20 sccm) and argon (5 sccm) flow with a 15 mTorr chamber pressure and a 50 W RF power for different durations (from 5 to 12.5 min). The silica colloidal templates were then wet-etched by hydrofluoric acid (2 vol %) in an ethanol solution, followed by drying under ambient conditions.

Characterization. Photographic images and scanning electron microscopy (SEM) images of the specimens were performed by a digital camera (EOS 805D, Canon) and a FEG-SEM (6335F, JEOL), respectively. The specimens were sputtered with a 5 nm-thick

platinum layer using a sputter coater (Agar Scientific) before SEM imaging. Optical reflectance and transmittance spectra of the specimens were characterized using a UV–vis–NIR spectrometer (HR4000, Ocean Optics) with a halogen-tungsten light source (LS-1, Ocean Optics). The reference spectra acquired from an aluminum-sputtered silicon standard (STAN-SSH, Ocean Optics) and a low-reflectivity glass standard (STAN-SSL, Ocean Optics) were applied in calibrating absolute reflectances. Average reflectance and average transmittance in the visible wavelength region were calculated by averaging measurements from five different areas of the specimen.

■ RESULTS AND DISCUSSION

Blue-tailed forest hawk dragonflies (*Orthetrum triangulare*) are conspicuous with their azure blue tails and highly transparent wings. The dragonfly wings exhibit high clarity even for wide viewing angles (Figure 1a,b). The optical transparency as evidenced is further assessed by evaluating average optical reflectances and average optical transmittances of the wings in the wavelength region from 380 to 800 nm at various incident angles (Figure 1c). It is found that the average reflectance is 7% at normal incidence (0°) and only increased by 8% as the incident angle reaches 75°. In contrast to that, the average transmittance slightly decreases from 91 to 83% while the angle of incidence varies from 0 to 75°. The broad-band omnidirectional antireflection behaviors originate from disorderedly arranged submicrometer-scale irregular conical structures on the wing membrane surface (Figure 1d). Interestingly, the conical structures are randomly arranged and randomly directed inclined. Besides this, it is observed that the base diameter of conical structures varies from 90 and 190 nm.

Inspired by the blue-tailed forest hawk dragonfly wings, non-close-packed inclined conical structures are engineered through integrating a scalable spin-coating technique and a colloidal lithography methodology (Figure 2). As shown in the schematic outline, silica colloids are shear-aligned into a non-close-packed arrangement on a shape memory polymer (poly(ETPTA)/poly(EGDA))-coated PET substrate in the spin-coating procedure. With a great etching selectivity toward the polymer relative to silica, the self-assembled silica colloids are exploited as plasma etching masks in an oxygen and argon plasma etching procedure for patterning pawn-like structure arrays. The pawn-like structures comprised silica colloids at the top and polymeric conical structures at the bottom, whose size and shape are determined by the silica colloid size and RIE operating parameters. For a long RIE duration, the conical structures are too thin to fully support the top colloids, bringing about the conformation of randomly inclined brown clamshell mushroom-like structure arrays. The top silica
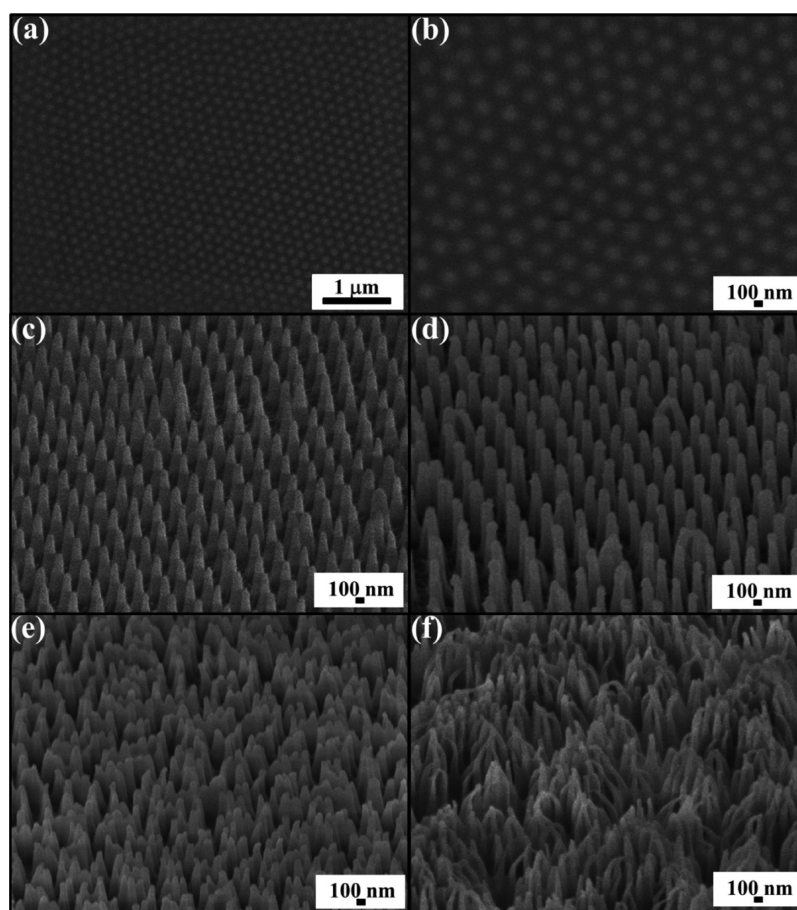
Figure 3. (a) Top-view SEM image of a spin-coated 190 nm silica colloidal crystal/polymer composite. (b) Magnified top-view SEM image of (a). Tilted-view SEM images of shape memory polymer-based conical structures templated from 190 nm silica colloidal crystals after different RIE durations of (c) 5, (d) 7.5, (e) 10, and (f) 12.5 min.

colloids are finally wet-etched using a hydrofluoric acid solution, leaving behind a non-close-packed shape memory polymer-based inclined conical structures with tunable geometries.

To investigate antireflection characteristics of the dragonfly wing-inspired structures, a monolayer of spin-coated 190 nm silica colloids is applied to fabricate inclined conical structures. It is evident that the silica colloid crystals are hexagonal non-close-packed and with a mean inter-colloid spacing of about 100 nm (Figure 3a,b). In the process of plasma etching [O_2 (15 sccm)/Ar (5 sccm)], the silica colloidal crystals are capable of preventing the polymer underneath them from being etched. After wet-etching the silica colloids, non-close-packed polymeric conical structure arrays are well-retained on the substrate (Figure 3c−f). The base diameter of the conical structures is 190 nm, while the structure height increases with longer RIE duration. Even though the shrinkage of silica colloids can be disregarded, the presence of isotropic oxygen plasma etching causes the configuration of sharp conical structures. After RIE for 7.5 min, the conical structure tips are too sharp to fully support the above colloids and therefore are randomly directed bended (Figure 3e). Importantly, the non-close-packed arrangement of periodic structures provides sufficient interspace to construct inclined structure arrays. For extending the RIE treatment beyond 10 min, the conical structure height is further increased, and the resultant conical structure tips are getting even sharper (Figure 3d). The sharp

structures with high aspect ratios, defined as a height/base diameter, are seriously bent and randomly bunched into collapsed bundles over large areas. The observed bundles are attributed to van der Waals forces between the neighboring bended conical structures.[46,47]

As demonstrated in previous study, non-close-packed subwavelength conical structure arrays fabricated by colloidal lithography can establish a refractive index gradient on the surface to suppress optical reflection at normal incidence, mimicking the antireflection mechanism of cicada wings.[48] To assess the antireflective characteristics of the dragonfly wing-inspired inclined structures, normal-incidence optical reflectance spectra of the inclined conical structure arrays templated from 190 nm silica colloids with various RIE durations are compared in Figure 4a. The bare PET film used in this work presents an average reflectance of 12% for wavelengths from 380 to 800 nm, confirming with the previous study.[48] The optical reflectance is reduced by creating incline conical structure arrays on the PET substrate. Obviously, the broad-band antireflection performance improves with the RIE duration, indicating that the optical reflection can be suppressed more efficiently through engineering incline conical structures with higher aspect ratios. Theoretically, the optical transmissions of the conical structure-covered substrates shall therefore be enhanced with increasing RIE durations. However, it is noticed that the spectral transmittances of the substrates with RIE treatments beyond 10 min are even lower
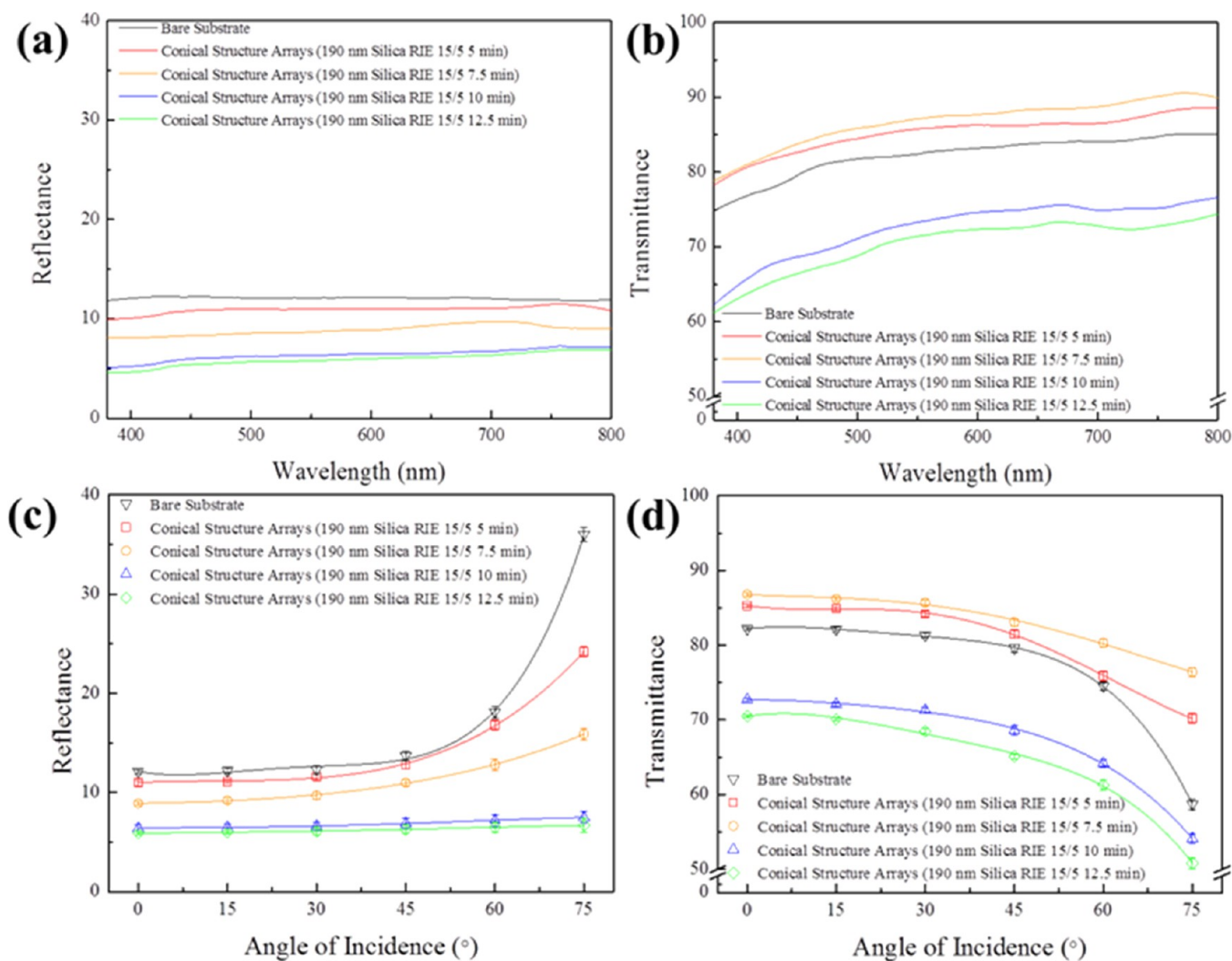
Figure 4. (a) Optical reflectance spectra and (b) optical transmittance spectra acquired from a bare PET substrate and PET substrates coated with shape memory polymer-based conical structures, which are templated from 190 nm silica colloidal crystals after different RIE durations at normal incidence. (c) Average optical reflectances and (d) average optical transmittances in the visible wavelength region acquired from a bare PET substrate and PET substrates coated with the conical structures at various incident angles.

than that of the bare substrate (Figure 4b). The diminished optical transmissions result from the formation of wide-ranging bundled conical structures, which are with the micrometer scale (Figure 3e,f). Consequently, part incident visible light is reflected or refracted within the collapsed bundles. To further comprehend the omnidirectional antireflection characteristics under the influence of inclined conical structures, average optical reflectances and transmittances in the visible wavelength region are acquired from the above-mentioned specimens at different incident angles. As shown in Figure 4c, despite the fact that the average optical reflectances increase while the angle of incidence varies from 0 to 75°, the reflectances are reduced by introducing inclined conical structures with longer RIE treatments. It is notable that the optical reflection can be suppressed even stronger for large incident angles. The average optical transmittances exhibit similar evolution trends with the average optical transmittances (Figure 4d). Although the collapsed bundle-covered substrates exhibit much lower average transmittances, it is evident that the optical transmission of the substrate at large incident angles can be greatly enhanced through engineering inclined conical structure arrays on the surface. In comparison with the bare

substrate, the 7.5 min RIE-treated conical structure-covered substrate displays 5% higher average transmittance at 0° and 18% higher average transmittance at 75°. The results disclose that inclined conical structures play an important role in designing and constructing broad-band omnidirectional antireflection coatings.

The effects of inclined structure shapes on the omnidirectional antireflection characteristics are systemically investigated in the study. Spin-coated 140 nm silica colloids and 90 nm silica colloids are served as structural templates, respectively, to pattern non-close-packed inclined conical structures with different aspect ratios (Figures S1 and S2). It is observed that the conical structures templated from either 140 or 90 nm silica colloids with 7.5 min RIE treatments are bended, whereas the conical structures with RIE treatments beyond 10 min are bunched into collapsed bundles. Compared to the conical structures templated from 190 nm silica colloids (Figure 3), conical structures with higher aspect ratios are manufactured by introducing smaller templating silica colloids for the reason that the base diameter of conical structures is proportional to the structural template size. The sharp structures are incapable of supporting the above structural templates, resulting in the
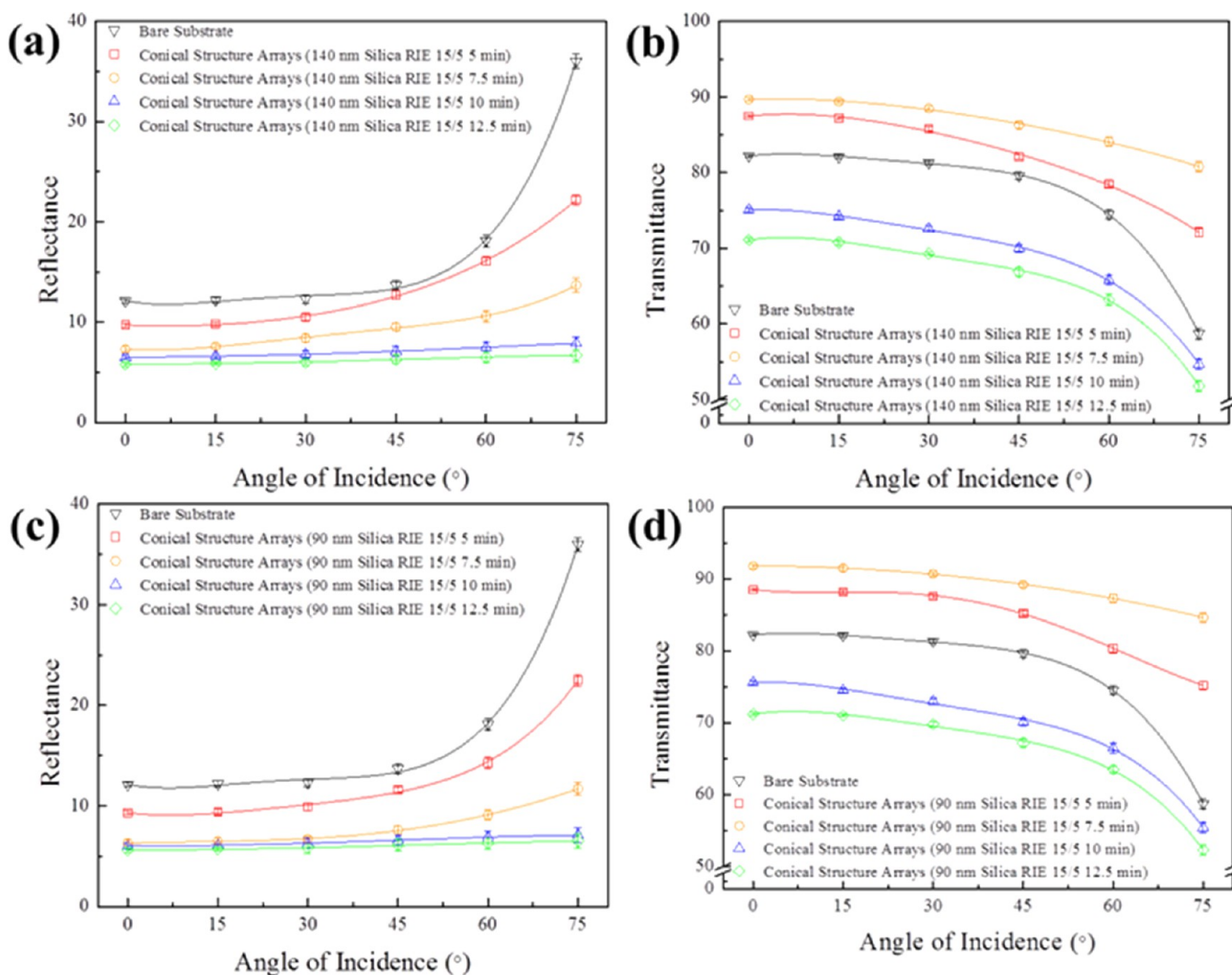
Figure 5. (a) Average optical reflectances and (b) average optical transmittances in the visible wavelength region acquired from a bare PET substrate and PET substrates coated with shape memory polymer-based conical structures, which are templated from 140 nm silica colloidal crystals after different RIE durations, at various incident angles. (c) Average optical reflectances and (d) average optical transmittances in the visible wavelength region acquired from a bare PET substrate and PET substrates coated with shape memory polymer-based conical structures, which are templated from 90 nm silica colloidal crystals after different RIE durations, at various incident angles.

formation of seriously inclined conical structures. Afterward, the average optical reflectances and transmittances in the visible wavelength region are evaluated from the conical structure arrays at various incident angles (Figure 5). Similar to the results as shown in Figure 4, the average reflectances at various incident angles decrease with the increase of RIE duration, while the average transmittances at various incident angles achieve maximum values as the RIE duration reaches 7.5 min. In addition, the average transmittances of the specimens with more than 10 min of RIE treatments are significantly decreased, caused by light scattering from the bundled structures. Importantly, the average transmittance of the substrate can be increased by 8% at 0° and 22% at 75° through engineering the inclined structures templated from 140 nm silica colloids (orange curve), while the inclined structures templated from 90 nm silica colloids can further enhance optical transmission by 10% at 0° and 25% at 75° (orange curve). The results reveal that the seriously inclined conical structures with higher aspect ratios establish smoother refractive index transitions at various angles of incidences and

therefore improve the omnidirectional antireflection performance.

For creating conical structures with even more serious inclinations, etching gas flow rates are also adjusted in the study. The RIE procedure is carried out using a mixture of oxygen and argon, in which the oxygen flow rate is varied from 10 to 20 sccm and the argon flow rate is fixed at 5 sccm (Figure S3). Figure 6a−c shows the SEM images of structure arrays templated from 190 nm silica colloids, which are etched in the presence of various oxygen/argon mixtures for 7.5 min. It is apparent that the conical structure height increases with higher oxygen flow rate, whereas the structure base diameter decreases slightly. Besides that, the sidewalls of the templated structures fabricated with a lower oxygen/argon flow ratio (10 sccm/5 sccm) are nearly vertical (Figure 6a). By contrast, seriously inclined conical structures with sharp tips have been achieved as the oxygen/argon flow ratio reaches 20 sccm/5 sccm (Figure 6c). It is found that variation in the oxygen flow rate affected the structural morphologies significantly. It is believed that the configuration of inclined conical structures is primarily caused by isotropic oxygen plasma etching on the
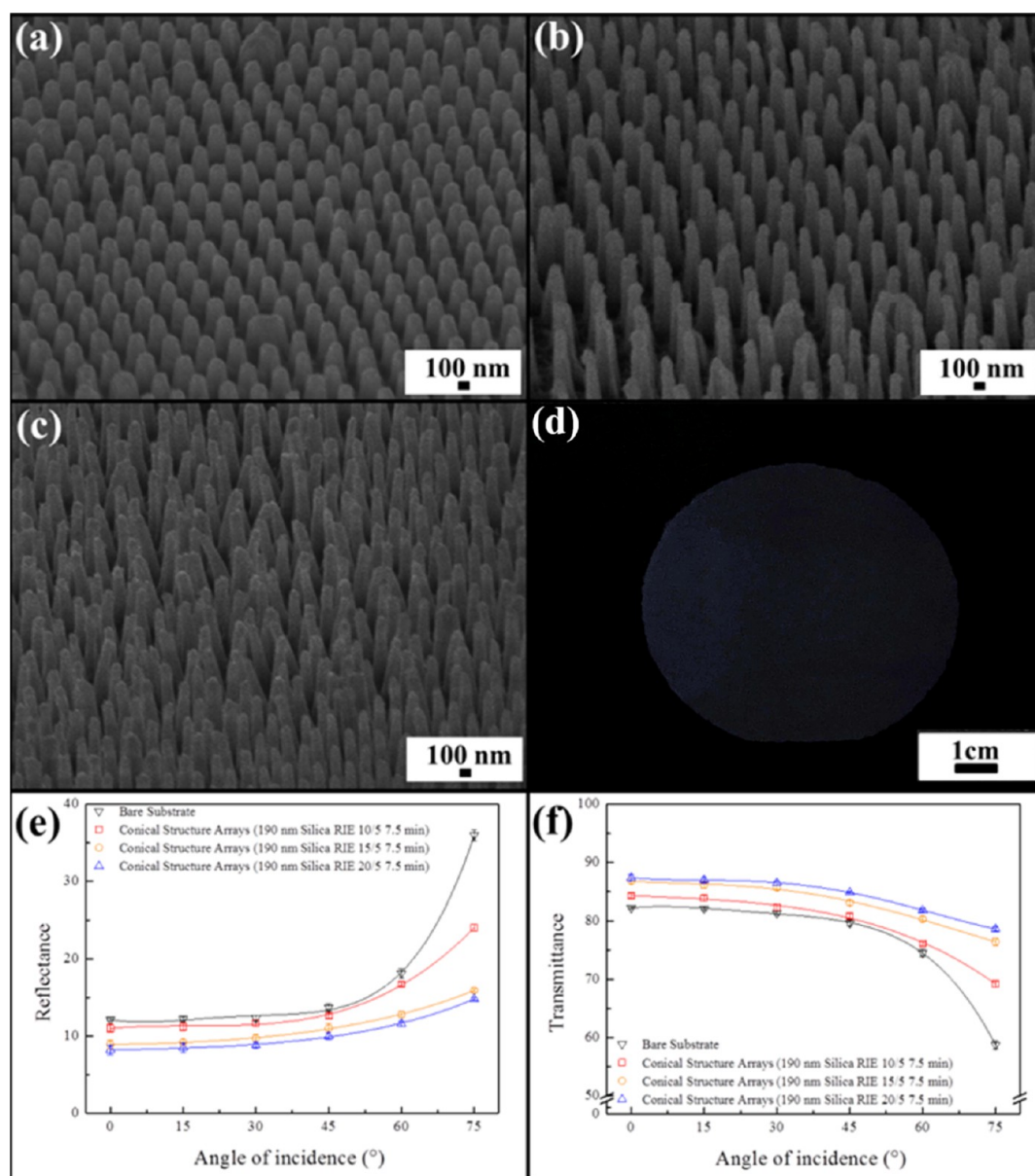
Figure 6. Tilted-view SEM images of PET substrates coated with shape memory polymer-based conical structures, which are templated from 190 nm silica colloidal crystals after 7.5 min RIE treatments with different RIE parameters of (a) O_2 (10 sccm)/Ar (5 sccm), (b) O_2 (15 sccm)/Ar (5 sccm), and (c) O_2 (20 sccm)/Ar (5 sccm). (d) Photographic image of the specimen in (c). (e) Average optical reflectances and (f) average optical transmittances in the visible wavelength region acquired from the specimens in (a–c) at various incident angles.

sidewalls of the templated structures during the RIE procedure. Interestingly, the seriously inclined conical structure-covered substrate is with high transparency and appears slightly blue in color, which is induced by light scattering from the templated structures (Figure 6d). The resulting light scattering greatly impairs the omnidirectional antireflection characteristics. As revealed in Figure 6e,f, the average reflectance is decreased by only 2% (blue curve), while the average transmittance is also increased by 2% (blue curve) as the oxygen flow rate is varied from 15 to 20 sccm.

To minimize the effects of light scattering, conical structure arrays are templated from 140 nm silica colloids and 90 nm silica colloids, respectively, in the presence of various oxygen/argon mixtures for 7.5 min (Figures S4 and S5). Similar to the above-mentioned results, heights and inclinations of the templated structures increase with the increase of oxygen

flow rate (Figures S4a–c, S5a–c). Compared with the structures templated from 190 nm silica colloids (Figure 6), sharper conical structures with greater inclinations are constructed by applying smaller silica colloids as structural templates. It is evident that the seriously inclined conical structures, templated from 140 nm silica colloidal crystals using an oxygen/argon flow ratio of 20 sccm/5 sccm, can efficiently suppress optical reflection even at large incident angles (Figure 7a). Importantly, the sharper conical structure tips result in less visible light scattering and therefore improve the optical transparency (Figure S4d). In comparison with a featureless substrate, the as-fabricated specimen exhibits 9% higher average transmittance at 0° and 27% higher average transmittance at 75° (Figure 7b). As expected, the inclined conical structures, templated from 90 nm silica colloidal crystals using the same oxygen/argon flow ratio, can further reduce the
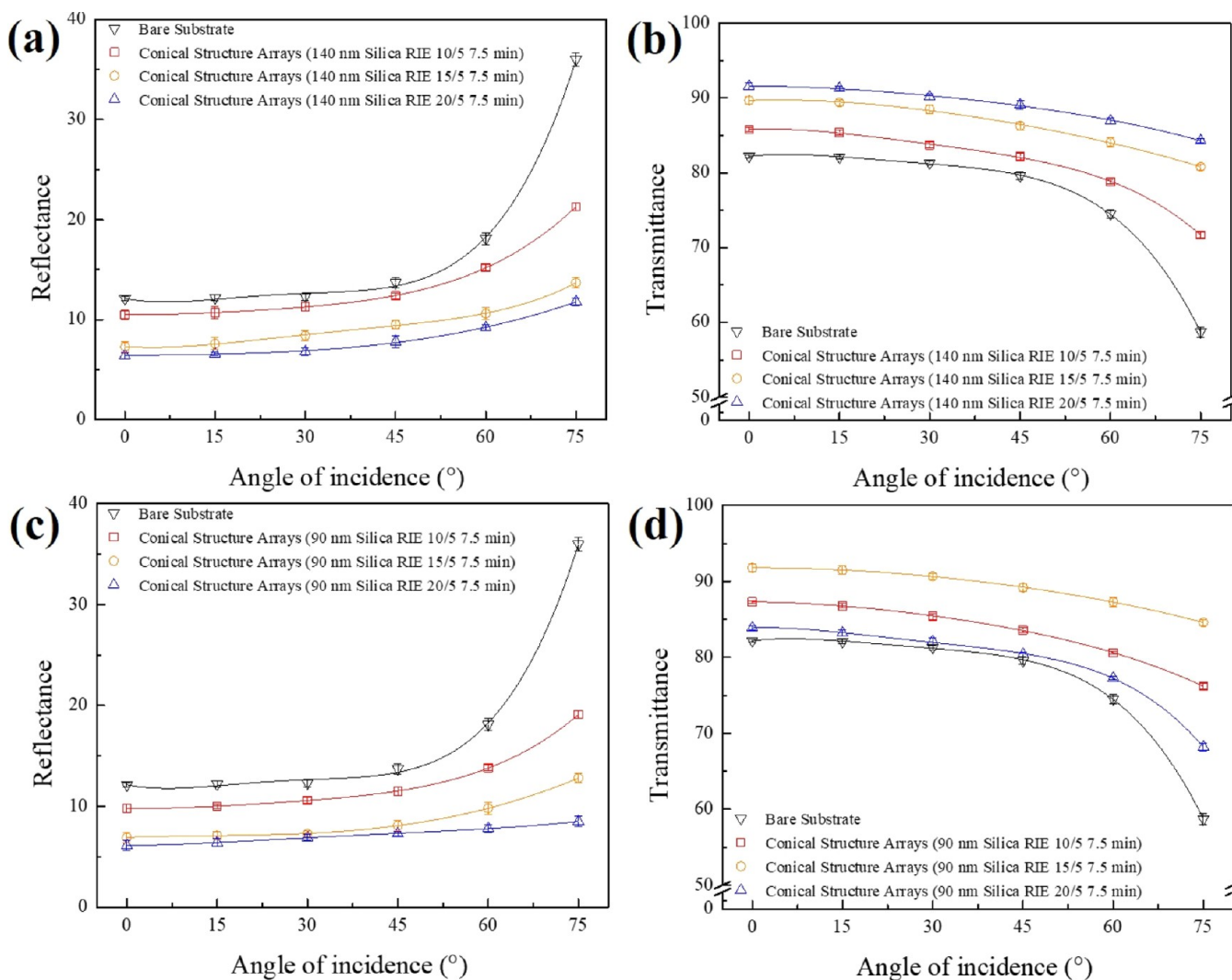
Figure 7. (a) Average optical reflectances and (b) average optical transmittances in the visible wavelength region acquired from a bare PET substrate and PET substrates coated with shape memory polymer-based conical structures, which are templated from 140 nm silica colloidal crystals after 7.5 min RIE treatments with different RIE parameters, at various incident angles. (c) Average optical reflectances and (d) average optical transmittances in the visible wavelength region acquired from a bare PET substrate and PET substrates coated with shape memory polymer-based conical structures, which are templated from 90 nm silica colloidal crystals after 7.5 min RIE treatments with different RIE parameters, at various incident angles.

average reflectances at various incident angles (Figure 7c). Nevertheless, the average transmittances at various incident angles of the specimen are only slightly higher than those of a featureless substrate (Figure 7d). We speculate that the optical transmission has been hindered by light scattering from the templated structure array (Figure S5c). It is noticed that the inter-structure distances of the inclined conical structures templated from nanometer-scale structural templates are less than 100 nm. The combination of seriously inclined conical structures and small inter-structure distances brings about the formation of bundled conical structures and consequently generates light scattering. In contrast to that, less inclined conical structures are templated from 90 nm silica colloidal crystals using an oxygen/argon flow ratio of 15 sccm/5 sccm. The as-engineered specimen is with low-haze and high transparency (Figure S5d), of which the average transmittance is 91% at 0° and decreased by only 5% at 75°. The results suggest that both structural configuration and inter-structure distance play important roles in determining omnidirectional antireflection characteristics.

Dragonfly wings behave broad-band omnidirectional antireflection properties originated from inclined irregular conical structures covering the wing surface. The irregularity is not only limited to the structure height but also the structure arrangement. To biomimic the disorderedly arranged structures, a monolayer of 190 nm silica colloids/140 nm silica colloids/90 nm silica colloids is spin-coated on a PET substrate, followed by plasma etching using various oxygen/argon mixtures for 7.5 min (Figure S6). As shown in Figure S7a,b, the silica colloids are randomly packed and with an average inter-colloid distance of less than 100 nm. After plasma etching and wet etching treatments, randomly directed inclined conical structures with base diameters of 190, 140, and 90 nm are established (Figure S7c−e). Clearly, seriously inclined conical structures without collapsed bundles are engineered as the oxygen/argon flow ratio reaches 15 sccm/5 sccm. It is worthwhile to note that the randomly packed structural templates provide adequate space for patterning inclined irregular structures. The dragon wing-inspired structure-covered substrate is highly transparent (Figure S7f) and
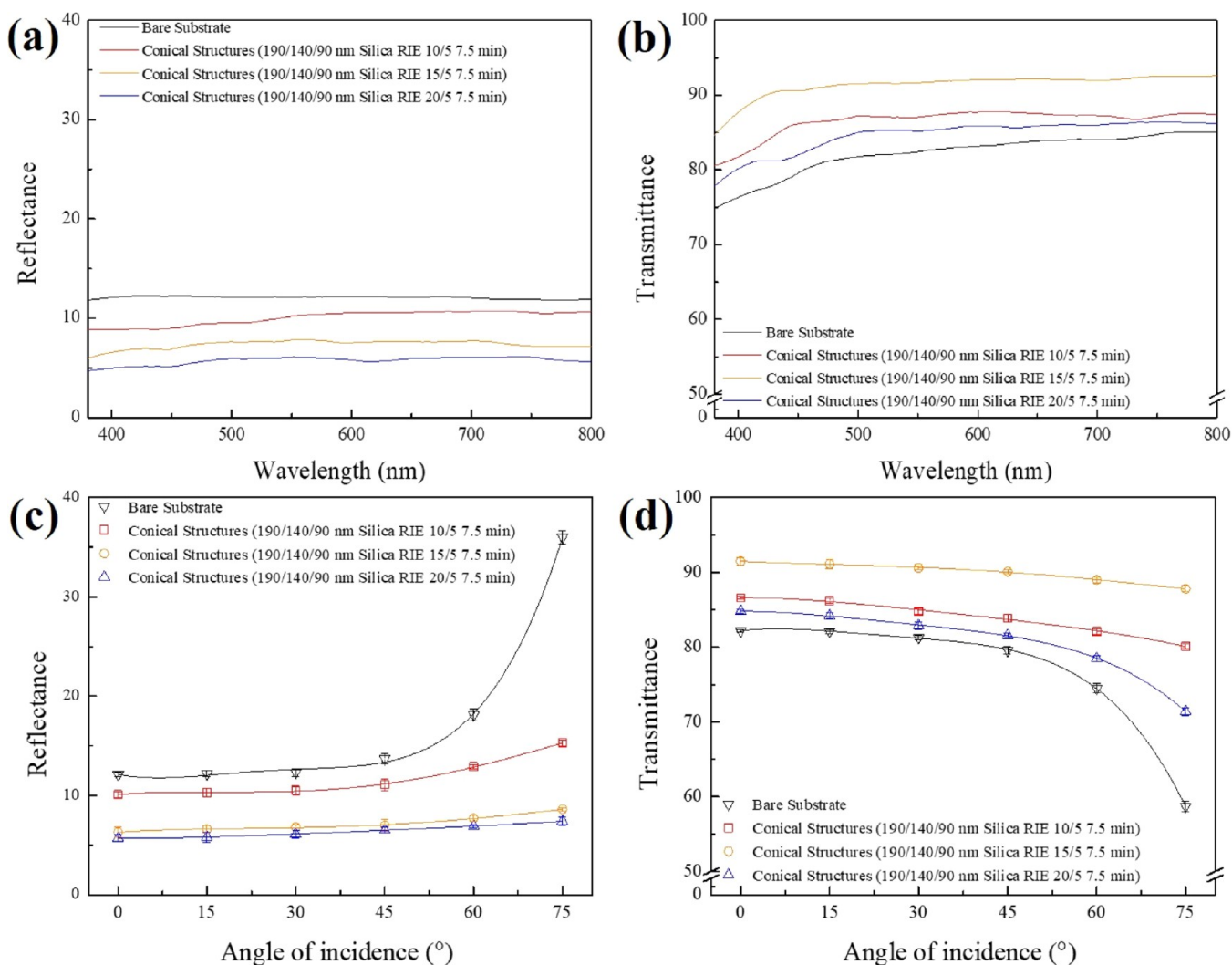
Figure 8. (a) Optical reflectance spectra and (b) optical transmittance spectra acquired from a bare PET substrate and PET substrates coated with shape memory polymer-based conical structures, which are templated from 190 nm silica colloids/140 nm silica colloids/90 nm silica colloids after 7.5 min RIE treatments with different RIE parameters, at normal incidence. (c) Average optical reflectances and (d) average optical transmittances in the visible wavelength region acquired from a bare PET substrate and PET substrates coated with the conical structures at various incident angles.

exhibits broad-band antireflection performance (Figure 8a,b). The average reflectance can be decreased from 12 to 6% at 0° and greatly decreased from 36 to 8% at 75° by applying the inclined irregular conical structures (Figure 8c). In addition, the average transmittances significantly improved as the incident angle varies from 0 to 75°. Figure 8d discloses that the average transmittance in the visible wavelength region reaches 92% at 0° and 89% at 75°. Most importantly, in comparison with the optical performances of the above-mentioned inclined conical structure arrays, omnidirectional antireflection performance is further improved through engineering the inclined irregular conical structures. The optical transmission of this inclined irregular conical structure-covered substrate only reduces slightly even at 75°. It is believed that irregular conical structures templated from different sized structural templates are with various inclinations and therefore lead to less bundled conical structures. The photographic images of a bare substrate and the dragon wing-inspired structure-covered substrate taken at 0, 30, and 60° are further compared in Figure S8. It is evident that the bare substrate displays a milky coloration for all the viewing angles.

The Fresnel's reflection is greatly suppressed by the inclined irregular conical structures. The dragon wing-inspired structure-covered substrate is highly transparent, and the letters underneath the specimen are clearly visible even as the viewing angle varies from 0 to 60°. By contrast, the substrates covered with inclined conical structure arrays, templated from various silica colloidal crystals, turn milky at large viewing angles (Figures S9–S11).

The poly(ETPTA)/poly(EGDA) composite-based structures can be deformed and then returned from the deformed shapes to their original shapes induced by external stimuli under ambient conditions.[30,49] The unique shape memory characteristics allow transitions between inclined conical structures and collapsed bundles and provide a platform to realize tunable antireflection coatings. Interestingly, the dragon wing-inspired structure-covered substrate becomes translucent after submerging the specimen in deionized water, followed by drying out of the water (Figure 9a). The dominancy of considerable water evaporation-induced capillary force over the polymer elasticity results in the observed collapsed bundles (Figure 9b), while van der Waals forces between neighboring
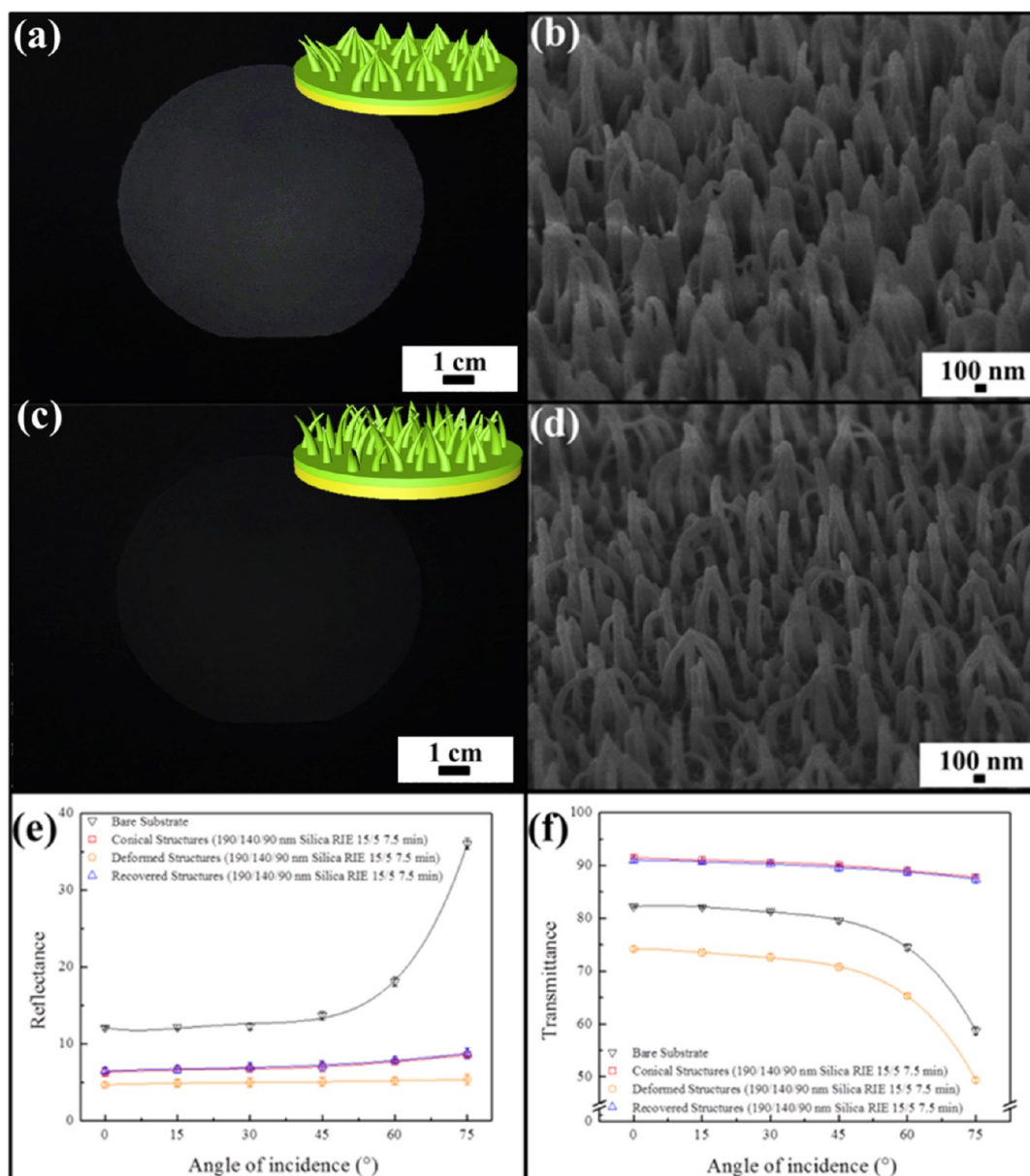
Figure 9. PET substrate coated with shape memory polymer-based conical structures, which are templated from 190 nm silica colloids/140 nm silica colloids/90 nm silica colloids after a 7.5 min RIE treatment with O_2 (15 sccm)/Ar (5 sccm). (a) Photographic image of the specimen dried out of water. (b) Tilted-view SEM image of the specimen in (a). (c) Photograph of the deformed specimen in (a) dried out of ethanol. (d) Tilted-view SEM image of the specimen in (c). (e) Average optical reflectances and (f) average optical transmittances in the visible wavelength region acquired from the deformed specimen and the recovered specimen at various incident angles.

bundled conical structures retain the adhered configuration after drying. Light scattering from the resultant bundles therefore leads to the pale white appearance. By contrast, the specimen turns into transparent subsequent to an ethanol drying procedure (Figure 9c). On account of the weak ethanol evaporation-induced capillary force, the temporarily deformed structures can be recovered to their original configuration by drying the collapsed bundles out of ethanol (Figure 9d). Besides ethanol, the recovery can also be triggered by drying out of varieties of solvents with low surface tensions. During the shape recovery, the solvents are absorbed into the shape memory polymer-based structures, relaxing the stretched polymer chains and increasing their mobility. As a result, entropy elasticity drives the bundled conical structures to recover their original configurations after drying out of

solvents.[50,51] The deformed structure-covered specimen and the recovered structure-covered specimen in the shape memory cycle possess drastically different antireflection characteristics depending on their corresponding structural configurations (Figure 9e,f). The deformed specimen exhibits low average optical reflectance and transmittance in the visible wavelength region caused by light scattering. In sharp contrast, the average transmittances of the recovered specimen are significantly improved at various incident angles. Its broadband omnidirectional antireflection performance matches with that of the undeformed specimen, revealing that the temporarily deformed structures return to their original configurations. Importantly, the capillary force-induced shape memory cycle is reversible, and the corresponding antireflection functionality can be switched for at least 25 cycles
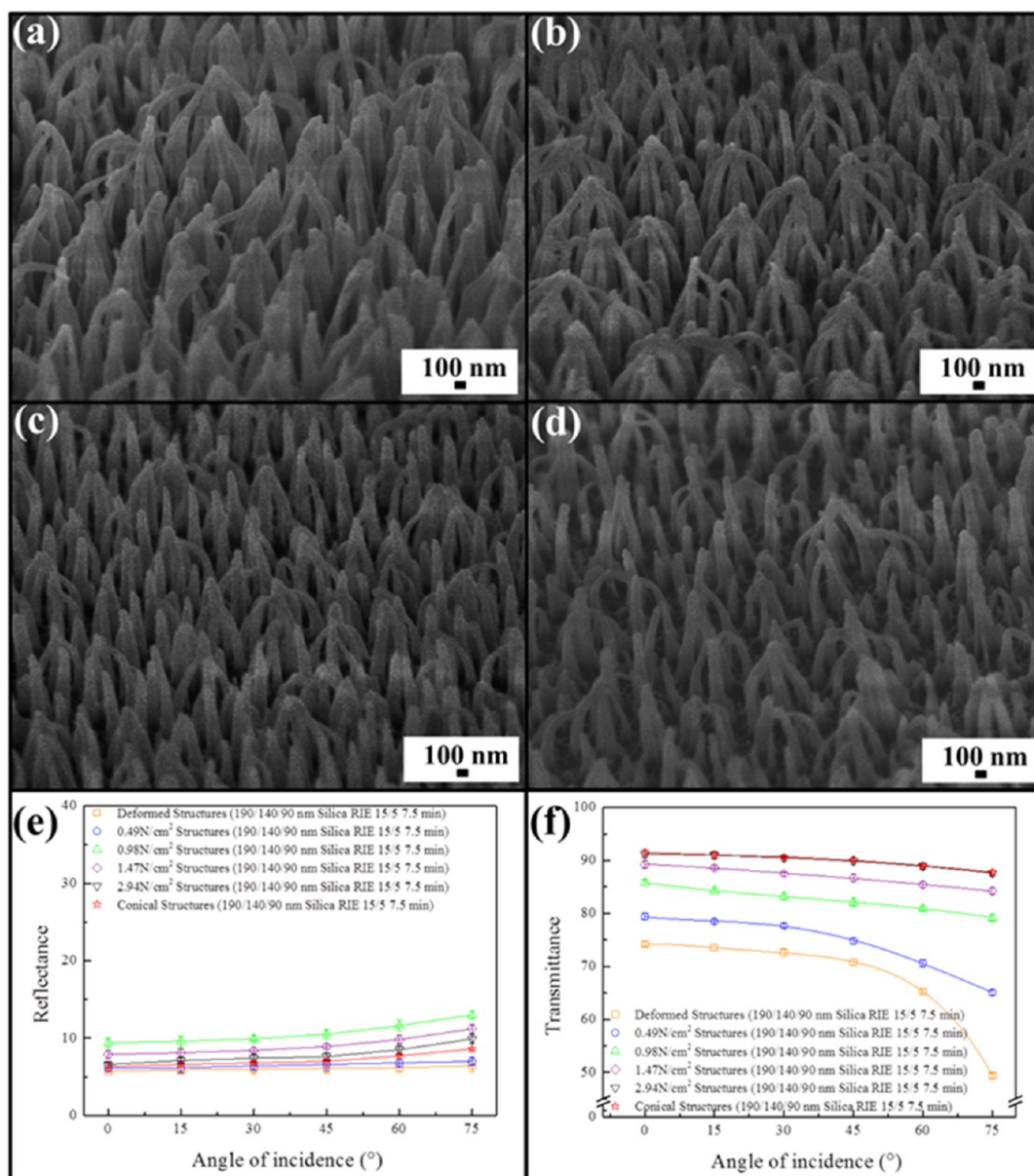
Figure 10. Tilted-view SEM images of a PET substrate coated with deformed shape memory polymer-based conical structures, which are templated from 190 nm silica colloids/140 nm silica colloids/90 nm silica colloids after a 7.5 min RIE treatment with O_2 (15 sccm)/Ar (5 sccm), under applying different contact pressures of (a) 0.49, (b) 0.98, (c) 1.47, and (d) 2.94 N/cm². (e) Average optical reflectances and (f) average optical transmittances in the visible wavelength region acquired from the deformed specimen and the recovered specimen at various incident angles.

(Figure S12). The results suggest that tunable antireflection coatings inspired by dragonfly wings are realized by applying solvent stimulations. Although a variety of elastic materials, such as elastomers and hydrogels, for fabricating switchable antireflective structures have been demonstrated, the temporary structures are not stable at ambient conditions and cannot be memorized for a long period of time.[52−54]

Even more importantly, the structural recovery can also be triggered in response to contact pressures. The external energy in the form of pressure is transferred to the collapsed bundles, during which the internal energy of the stretched shape memory polymer chains increases. The increased internal energy allows the deformed structures to overcome the shape memory activation barrier and trigger the conical structure recovery. To evaluate the critical contact pressure needed to achieve the structural recovery, different weights are placed on

the collapsed structure-covered substrate in a specific area. It is in accordance with intuition that the higher the contact pressure, the more the temporarily bundled structures are recovered, as verified in Figure 10a−d. In addition, the SEM images disclose that the inclined irregular conical structures are fully recovered as the applied contact pressure reaches 2.94 N/cm². It is worthwhile to emphasize that higher contact pressures lead to less collapsed bundles, which is associated with better antireflection performance. As a result, the average optical reflectance gradually decreases, whereas the average optical transmittance gradually increases with increasing contact pressures (Figure 10e,f). The average transmittance is improved from 80 to 92% at 0° and significantly improved from 65 to 89% at 75° as the applied contact pressure is varied from 0.49 to 2.94 N/cm². The results reveal that the broadband omnidirectional antireflection characteristics of the shape

memory polymer-based inclined conical structures can be adjusted by applying different contact pressures. Besides that, it is evident that the average transmittances of the specimen under 2.94 N/cm² contact pressure match well with those of the original specimen, further demonstrating that the deformed structures are fully recovered. As evidenced by previous results, the recovered antireflection characteristics can once again be eliminated by drying out of water. The contact pressure-induced antireflection performance is therefore tunable and well maintained after switching for more than 25 shape memory cycles (Figure S13). Moreover, the poly(ETPTA)/poly(EGDA) composite-based conical structures are flexible and can maintain their antireflection characteristics under bending. The deterioration of antireflection is not found even as the bending angle is increased up to 45° (Figures 8 and S14). Importantly, the antireflection characteristics can be fully recovered after bending for 25 times. The results indicate that the conical structures can serve as an effective antireflective layer in the bending mode as well.

CONCLUSIONS

To conclude, blue-tailed forest hawk dragonfly wing-inspired tunable antireflection coatings are engineered by integrating a colloidal lithography technology with stimuli-responsive shape memory polymers. In comparison with moth eye-like conical structure arrays, the optimized inclined irregular conical structures establish smoother refractive index gradients at various angles of incidences, leading to impressive broad-band omnidirectional antireflection performance. Importantly, the antireflection characteristics can be eliminated through deforming the intrinsic structures, triggered by water evaporation-induced capillary forces. The temporarily deformed structures and the corresponding antireflection characteristics can then be recovered by drying the structures out of ethanol or applying external contact pressures in ambient environments. The switchable stimuli-responsive shape memory cycle, associated with the tunable broad-band omnidirectional antireflection functionality, adds new dimensions to various existing and future optical and optoelectronic devices.

ASSOCIATED CONTENT

Ⓢ Supporting Information

The Supporting Information is available free of charge at https://pubs.acs.org/doi/10.1021/acs.langmuir.1c01341.

> SEM images, photographic images, and fabrication procedures of various inclined conical structures and tunable antireflection characteristics of a PET substrate coated with shape memory polymer-based inclined conical structures enabled by applying solvent stimulations and contact pressures (PDF)

AUTHOR INFORMATION

Corresponding Authors

Kun-Yi Andrew Lin − *Department of Environmental Engineering, National Chung Hsing University, Taichung City 40227, Taiwan*; Email: linky@nchu.edu.tw

Hongta Yang − *Department of Chemical Engineering, National Chung Hsing University, Taichung City 40227, Taiwan;* ⓘ orcid.org/0000-0002-5822-1469; Email: hyang@dragon.nchu.edu.tw

Authors

Yu-Han Chen − *Department of Chemical Engineering, National Chung Hsing University, Taichung City 40227, Taiwan*

Huei-Yin Chen − *Department of Chemical Engineering, National Chung Hsing University, Taichung City 40227, Taiwan*

Chung-Jui Lai − *Department of Chemical Engineering, National Chung Hsing University, Taichung City 40227, Taiwan*

Jung-Hsuan Hsu − *Department of Chemical Engineering, National Chung Hsing University, Taichung City 40227, Taiwan*

Complete contact information is available at:
https://pubs.acs.org/10.1021/acs.langmuir.1c01341

Notes
The authors declare no competing financial interest.

REFERENCES

(1) Yu, F.; Zhang, Q.; Thedford, R. P.; Singer, A.; Smilgies, D.-M.; Thompson, M. O.; Wiesner, U. B. Block Copolymer Self-Assembly-Directed and Transient Laser Heating-Enabled Nanostructures toward Phononic and Photonic Quantum Materials. *ACS Nano* **2020**, *14*, 11273−11282.

(2) Montgomery, G. P., Jr. Antireflection Coatings for Veiling Glare Reduction. *Opt. Eng.* **1982**, *21*, 216039.

(3) Bacon-Brown, D. A.; Braun, P. V. Tunable Antireflection Coating to Remove Index-Matching Requirement for Interference Lithography. *Adv. Opt. Mater.* **2018**, *6*, 1701049.

(4) Isakov, K.; Kauppinen, C.; Franssila, S.; Lipsanen, H. Superhydrophobic Antireflection Coating on Glass Using Grass-like Alumina and Fluoropolymer. *ACS Appl. Mater. Interfaces* **2020**, *12*, 49957−49962.

(5) Agustín-Sáenz, C.; Machado, M.; Tercjak, A. Polyfluoroalkyl-Silica Porous Coatings with High Antireflection Properties and Low Surface Free Energy for Glass in Solar Energy Application. *Appl. Surf. Sci.* **2020**, *509*, 144864.

(6) Li, Y.; Hu, K.; Han, X.; Yang, Q.; Xiong, Y.; Bai, Y.; Guo, X.; Cui, Y.; Yuan, C.; Ge, H. Phase Separation of Silicon-Containing Polymer/Polystyrene Blends in Spin-Coated Films. *Langmuir* **2016**, *32*, 3670−3678.

(7) Fardo, F. M.; Ribeiro, R.; Strauss, J. d. A.; Nardi, J.; Ferreira, L.; Schmökel, G.; Costa, T. M. H.; Pereira, M. B.; Horowitz, F. Double Layer SiO₂−TiO₂ Sol−Gel Thin Films on Glass for Antireflection, Antifogging, and UV Recoverable Self-Cleaning. *Appl. Opt.* **2020**, *59*, 7720−7725.

(8) Kluska, S.; Hejduk, K.; Drabczyk, K.; Lipiński, M. Optical Properties and Passivation Effects of Silicon Nitride Three Layer Stacks Deposited by Plasma Enhanced Chemical Vapor Deposition. *Phys. Status Solidi A* **2016**, *213*, 1839−1847.

(9) Zhang, L.; Li, Y.; Sun, J.; Shen, J. Layer-by-Layer Fabrication of Broad-Band Superhydrophobic Antireflection Coatings in Near-Infrared Region. *J. Colloid Interface Sci.* **2008**, *319*, 302−308.

(10) Jia, G.; Ji, Z.; Wang, H.; Chen, R. Preparation and Properties of Five-Layer Graded-Refractive-Index Antireflection Coating Nano-structured by Solid and Hollow Silica Particles. *Thin Solid Films* **2017**, *642*, 174−181.

(11) Zou, X.; Tao, C.; Yan, L.; Yang, F.; Lv, H.; Yan, H.; Wang, Z.; Li, Y.; Wang, J.; Yuan, X.; Zhang, L. One-Step Sol-Gel Preparation of

Ultralow-Refractive-Index Porous Coatings with Mulberry-Like Hollow Silica Nanostructures. *Surf. Coat. Technol.* **2018**, *341*, 57−63.

(12) Krishnan, M. R.; Chien, Y.-C.; Cheng, C.-F.; Ho, R.-M. Fabrication of Mesoporous Polystyrene Films with Controlled Porosity and Pore Size by Solvent Annealing for Templated Syntheses. *Langmuir* **2017**, *33*, 8428−8435.

(13) Chi, F.; Zeng, Y.; Liu, C.; Liang, D.; Li, Y.; Xie, R.; Pan, N.; Ding, C. Aggregation of Silica Nanoparticles in Sol−Gel Processes to Create Optical Coatings with Controllable Ultralow Refractive Indices. *ACS Appl. Mater. Interfaces* **2020**, *12*, 16887−16895.

(14) Khan, S. B.; Wu, H.; Fei, Z.; Ning, S.; Zhang, Z. Antireflective Coatings with Enhanced Adhesion Strength. *Nanoscale* **2017**, *9*, 11047−11054.

(15) Tu, Y.-M.; Samineni, L.; Ren, T.; Schantz, A. B.; Song, W.; Sharma, S.; Kumar, M. Prospective Applications of Nanometer-Scale Pore Size Biomimetic and Bioinspired Membranes. *J. Membr. Sci.* **2021**, *620*, 118968.

(16) Gao, X.; Guo, Z. Biomimetic Superhydrophobic Surfaces with Transition Metals and Their Oxides: A Review. *J. Bionic Eng.* **2017**, *14*, 401−439.

(17) Xiang, T.; Hou, J.; Xie, H.; Liu, X.; Gong, T.; Zhou, S. Biomimetic Micro/Nano Structures for Biomedical Applications. *Nano Today* **2020**, *35*, 100980.

(18) Plettl, A.; Enderle, F.; Saitner, M.; Manzke, A.; Pfahler, C.; Wiedemann, S.; Ziemann, P. Non-Close-Packed Crystals from Self-Assembled Polystyrene Spheres by Isotropic Plasma Etching: Adding Flexibility to Colloid Lithography. *Adv. Funct. Mater.* **2009**, *19*, 3279−3284.

(19) Zhao, B.; Hu, M.; Ao, X.; Chen, N.; Pei, G. Radiative cooling: A Review of Fundamentals, Materials, Applications, and Prospects. *Appl. Energy* **2019**, *236*, 489−513.

(20) Cadiz, F.; Courtade, E.; Robert, C.; Wang, G.; Shen, Y.; Cai, H.; Taniguchi, T.; Watanabe, K.; Carrere, H.; Lagarde, D. Excitonic Linewidth Approaching the Homogeneous Limit in MoS_2-Based Van Der Waals Heterostructures. *Phys. Rev. X* **2017**, *7*, 021026.

(21) Tseng, H.-Y.; Chen, Y.-H.; Chen, R.-Y.; Yang, H. Reversibly Erasable Broadband Omnidirectional Antireflection Coatings Inspired by Inclined Conical Structures on Blue-Tailed Forest Hawk Dragonfly Wings. *ACS Appl. Mater. Interfaces* **2020**, *12*, 10883−10892.

(22) Wang, X.; Fang, Y.; Shi, B.; Huang, F.; Rong, F.; Que, R. Three-Dimensional $NiCo_2O_4$@ $NiCo_2O_4$ Core−Shell Nanocones Arrays for High-Performance Supercapacitors. *Chem. Eng. J.* **2018**, *344*, 311−319.

(23) Zuo, W.; Li, J.; Zhang, Y.; Li, Q.; Jia, S.; He, Z. Multi-Factor Impact Mechanism on Combustion Efficiency of a Hydrogen-Fueled Micro-Cylindrical Combustor. *Int. J. Hydrogen Energy* **2020**, *45*, 2319−2330.

(24) Li, X.; Zhu, M.; Du, M.; Lv, Z.; Zhang, L.; Li, Y.; Yang, Y.; Yang, T.; Li, X.; Wang, K. High Detectivity Graphene-Silicon Heterojunction Photodetector. *Small* **2016**, *12*, 595−601.

(25) Mohammadi, N.; Asadi, H.; Aghdam, M. M. An Efficient Solver for Fully Coupled Solution of Interaction between Incompressible Fluid Flow and Nanocomposite Truncated Conical Shells. *Comput. Methods Appl. Mech. Eng.* **2019**, *351*, 478−500.

(26) Banerjee, S.; Dionysiou, D. D.; Pillai, S. C. Self-Cleaning Applications of TiO_2 by Photo-Induced Hydrophilicity and Photo-catalysis. *Appl. Catal., B* **2015**, *176*, 396−428.

(27) Kasani, S.; Curtin, K.; Wu, N. A Review of 2D and 3D Plasmonic Nanostructure Array Patterns: Fabrication, Light Management and Sensing Applications. *Nanophotonics* **2019**, *8*, 2065−2089.

(28) Spinelli, P.; Verschuuren, M.; Polman, A. Broadband Omnidirectional Antireflection Coating Based on Subwavelength Surface Mie Resonators. *Nat. Commun.* **2012**, *3*, 692.

(29) Mourdikoudis, S.; Pallares, R. M.; Thanh, N. T. K. Characterization Techniques for Nanoparticles: Comparison and Complementarity Upon Studying Nanoparticle Properties. *R. Soc. Chem.* **2018**, *10*, 12871−12934.

(30) Leo, S.-Y.; Zhang, W.; Zhang, Y.; Ni, Y.; Jiang, H.; Jones, C.; Jiang, P.; Basile, V.; Taylor, C. Chromogenic Photonic Crystal Sensors

Enabled by Multistimuli-Responsive Shape Memory Polymers. *Small* **2018**, *14*, 1703515.

(31) Ivanova, E. P.; Hasan, J.; Webb, H. K.; Gervinskas, G.; Juodkazis, S.; Truong, V. K.; Wu, A. H.; Lamb, R. N.; Baulin, V. A.; Watson, G. S. Bactericidal Activity of Black Silicon. *Nat. Commun.* **2013**, *4*, 2838.

(32) Chakma, P.; Konkolewicz, D. Dynamic Covalent Bonds in Polymeric Materials. *Angew. Chem., Int. Ed.* **2019**, *58*, 9682−9695.

(33) Xue, J.; Wu, T.; Dai, Y.; Xia, Y. Electrospinning and Electrospun Nanofibers: Methods, Materials, and Applications. *Chem. Rev.* **2019**, *119*, 5298−5415.

(34) Sharma, K.; Arora, A.; Tripathi, S. Review of Supercapacitors: Materials and Devices. *J. Energy Storage* **2019**, *21*, 801−825.

(35) Huang, J.; Fan, J.; Cao, L.; Xu, C.; Chen, Y. A Novel Strategy to Construct Co-Continuous PLA/NBR Thermoplastic Vulcanizates: Metal-Ligand Coordination-Induced Dynamic Vulcanization, Balanced Stiffness-Toughness and Shape Memory Effect. *Chem. Eng. J.* **2020**, *385*, 123828.

(36) Sun, L.; Huang, W. M.; Ding, Z.; Zhao, Y.; Wang, C. C.; Purnawali, H.; Tang, C. Stimulus-Responsive Shape Memory Materials: A Review. *Mater. Des.* **2012**, *33*, 577−640.

(37) Liu, Y.; Du, H.; Liu, L.; Leng, J. Shape Memory Polymers and Their Composites in Aerospace Applications: A Review. *Smart Mater. Struct.* **2014**, *23*, 023001.

(38) Swain, B.; Mallick, P.; Gupta, R. K.; Mohapatra, S.; Yasin, G.; Nguyen, T.; Behera, A. Mechanical and Tribological Properties Evaluation of Plasma-Sprayed Shape Memory Alloy Coating. *J. Alloys Compd.* **2021**, *863*, 158599.

(39) Yan, B.; Zheng, X.; Tang, P.; Yang, H.; He, J.; Zhou, S. Investigating Switchable Nanostructures in Shape Memory Process for Amphipathic Janus Nanoparticles. *ACS Appl. Mater. Interfaces* **2018**, *10*, 36249−36258.

(40) Hsu, C.-C.; Lan, W.-L.; Chen, N.-P.; Wu, C.-C. The Hydrophobic and Omnidirectional Antireflection Coating of SiO_2 Nanospheres with C18-TEOS. *Opt. Laser Technol.* **2014**, *58*, 202−206.

(41) Ren, Z.; Jiang, H.; Liu, G.; Sun, Q. Antireflective Characteristics of Hemispherical Grid Grating. *Sci. Bull.* **2005**, *50*, 1309−1314.

(42) Meng, H.; Li, G. Reversible Switching Transitions of Stimuli-Responsive Shape Changing Polymers. *J. Mater. Chem. A* **2013**, *1*, 7838−7865.

(43) Shafranek, R. T.; Millik, S. C.; Smith, P. T.; Lee, C.-U.; Boydston, A. J.; Nelson, A. Stimuli-Responsive Materials in Additive Manufacturing. *Prog. Polym. Sci.* **2019**, *93*, 36−67.

(44) Liang, R.; Wang, L.; Yu, H.; Khan, A.; Amin, B. U.; Khan, R. U. Molecular Design, Synthesis and Biomedical Applications of Stimuli-Responsive Shape Memory Hydrogels. *Eur. Polym. J.* **2019**, *114*, 380−396.

(45) Stöber, W.; Fink, A.; Bohn, E. Controlled Growth of Monodisperse Silica Spheres in the Micron Size Range. *J. Colloid Interface Sci.* **1968**, *26*, 62−69.

(46) Zhao, H.; Yin, Y.; Zhong, Z. Micro and Nano Structures and Morphologies on the Wing Veins of Dragonflies. *Sci. Bull.* **2010**, *55*, 1993−1995.

(47) Wang, G.; Dai, Z.; Xiao, J.; Feng, S.; Weng, C.; Liu, L.; Xu, Z.; Huang, R.; Zhang, Z. Bending of Multilayer Van der Waals Materials. *Phys. Rev. Lett.* **2019**, *123*, 116101.

(48) Chen, Y.-C.; Huang, Z.-S.; Yang, H. Cicada-Wing-Inspired Self-Cleaning Antireflection Coatings on Polymer Substrates. *ACS Appl. Mater. Interfaces* **2015**, *7*, 25495−25505.

(49) Fang, Y.; Ni, Y.; Leo, S.-Y.; Wang, B.; Basile, V.; Taylor, C.; Jiang, P. Direct Writing of Three-Dimensional Macroporous Photonic Crystals on Pressure-Responsive Shape Memory Polymers. *ACS Appl. Mater. Interfaces* **2015**, *7*, 23650−23659.

(50) Salvekar, A. V.; Huang, W. M.; Xiao, R.; Wong, Y. S.; Venkatraman, S. S.; Tay, K. H.; Shen, Z. X. Water-Responsive Shape Recovery Induced Buckling in Biodegradable Photo-Cross-Linked Poly (Ethylene Glycol)(PEG) Hydrogel. *Acc. Chem. Res.* **2017**, *50*, 141−150.

(51) Löwenberg, C.; Balk, M.; Wischke, C.; Behl, M.; Lendlein, A. Shape-Memory Hydrogels: Evolution of Structural Principles to Enable Shape Switching of Hydrophilic Polymer Networks. *Acc. Chem. Res.* **2017**, *50*, 723−732.

(52) Chhajed, S.; Schubert, M. F.; Kim, J. K.; Schubert, E. F. Nanostructured Multilayer Graded-Index Antireflection Coating for Si Solar Cells with Broadband and Omnidirectional Characteristics. *Appl. Phys. Lett.* **2008**, *93*, 251108.

(53) Huang, Z.; Hawkeye, M. M.; Brett, M. J. Enhancement in Broadband and Quasi-Omnidirectional Antireflection of Nanopillar Arrays by Ion Milling. *Nanotechnology* **2012**, *23*, 275703.

(54) Zhu, X.; Wu, G.; Dong, R.; Chen, C.-M.; Yang, S. Capillarity Induced Instability in Responsive Hydrogel Membranes with Periodic Hole Array. *Soft Matter* **2012**, *8*, 8088−8093.